Radiology

CT-based Airway Flow Model to Assess Ventilation in Chronic Obstructive Pulmonary Disease: A Pilot Study

Minsuok Kim, PhD • Ozkan Doganay, PhD • Tahreema N. Matin, FRCR, DPhil • Thomas Povey, DPhill • Fergus V. Gleeson, FRCP, FRCR, FCCP

From the Departments of Engineering Science (M.K., T.P.) and Oncology (O.D., F.V.G.), University of Oxford, Parks Road, Oxford OX1 3PJ, England; and Department of Radiology, The Churchill Hospital, Oxford University Hospitals NHS Trust, Headington, England (O.D., T.N.M., F.V.G.). Received February 22, 2019; revision requested April 25; revision received August 6; accepted August 22. **Address correspondence to** M.K. (e-mail: *minsuok.kim@eng.ox.ac.uk*).

Study supported by Cancer Research UK (C5255), the Engineering and Physical Sciences Research Council in the UK (A16466), and the NIHR Biomedical Research Centre, Oxford.

Conflicts of interest are listed at the end of this article.

See also the editorial by Schiebler and Parraga in this issue.

Radiology 2019; 293:666–673 • https://doi.org/10.1148/radiol.2019190395 • Content code: CH

Background: The lack of functional information in thoracic CT remains a limitation of its use in the clinical management of chronic obstructive pulmonary disease (COPD).

Purpose: To compare the distribution of pulmonary ventilation assessed by a CT-based full-scale airway network (FAN) flow model with hyperpolarized xenon 129 (^{129}Xe) MRI (hereafter, ^{129}Xe MRI) and technetium 99m–diethylenetriaminepentaacetic acid aerosol SPECT ventilation imaging (hereafter, V-SPECT) in participants with COPD.

Materials and Methods: In this prospective study performed between May and August 2017, pulmonary ventilation in participants with COPD was computed by using the FAN flow model. The modeled pulmonary ventilation was compared with functional imaging data from breath-hold time-series ^{129}Xe MRI and V-SPECT. FAN-derived ventilation images on the coronal plane and volumes of interest were compared with functional lung images. Percentage lobar ventilation estimated by the FAN model was compared with that measured at ^{129}Xe MRI and V-SPECT. The statistical significance of ventilation distribution between FAN and functional images was demonstrated with the Spearman correlation coefficient and χ^2 distance.

Results: For this study, nine participants (seven men [mean age, 65 years ± 5 {standard deviation}] and two women [mean age, 63 years ± 7]) with COPD that was Global Initiative for Chronic Obstructive Lung Disease stage II–IV were enrolled. FAN-modeled ventilation profile showed strong positive correlation with images from ^{129}Xe MRI ($\rho = 0.67$; $P < .001$) and V-SPECT ($\rho = 0.65$; $P < .001$). The χ^2 distances of the ventilation histograms in the volumes of interest between the FAN and ^{129}Xe MRI and FAN and V-SPECT were 0.16 ± 0.08 and 0.28 ± 0.14, respectively. The ratios of lobar ventilations in the models were linearly correlated to images from ^{129}Xe MRI ($\rho = 0.67$; $P < .001$) and V-SPECT ($\rho = 0.59$; $P < .001$).

Conclusion: A CT-based full-scale airway network flow model provided regional pulmonary ventilation information for chronic obstructive pulmonary disease and correlates with hyperpolarized xenon 129 MRI and technetium 99m–diethylenetriaminepentaacetic acid aerosol SPECT ventilation imaging.

©RSNA, 2019

Online supplemental material is available for this article.

Chronic obstructive pulmonary disease (COPD) is a leading cause of mortality and morbidity with a substantial worldwide economic and social burden (1). By 2020, it is expected that COPD will rank third in terms of disease mortality and fifth for disease burden (2). Concerted efforts are being made to improve its diagnosis, stratify disease severity, and develop therapeutic treatments. This requires medical imaging techniques that are capable of providing reproducible and precise imaging biomarkers for determining the structural and functional abnormalities in the various COPD phenotypes.

Thoracic CT is a clinically established method for evaluating pulmonary structural abnormalities (eg, the presence and severity of emphysema in COPD) (3–5). Although CT is routinely used for structural assessment, it is weakly correlated with the forced expiratory volume in 1 second (6,7). Furthermore, the structural evaluation from CT does not predict the rate of decline of an individual's health or their COPD prognosis (8).

Technetium 99m–diethylenetriaminepentaacetic acid aerosol SPECT ventilation imaging (hereafter, V-SPECT) helps to obtain pulmonary functional information with the ability to depict different COPD phenotypes and help identify disease progression (9). Nonetheless, the routine use of V-SPECT in clinical practice is limited by its inherent low spatial resolution, patient's exposure to ionizing radiation, its availability, and the cost (10).

Hyperpolarized gas MRI is a noninvasive, ionizing radiation–free technique that uses the noble gases helium 3 or xenon 129 (^{129}Xe) (11–13). The technique enables detection of regional ventilation abnormalities in COPD through ventilation defects and apparent diffusion coefficients (14). Although hyperpolarized ^{129}Xe MRI (hereafter, referred to as ^{129}Xe MRI) ventilation offers high spatial and temporal resolutions compared

This copy is for personal use only. To order printed copies, contact *reprints@rsna.org*

Abbreviations

COPD = chronic obstructive pulmonary disease, FAN = full-scale airway network

Summary

By using CT images with routine pulmonary function testing, computation models demonstrated lung ventilation comparable to images obtained by using hyperpolarized xenon 129 MRI and technetium 99m–diethylenetriaminepentaacetic acid SPECT ventilation imaging.

Key Results

- Full-scale airway network (FAN) flow-modeled ventilation showed strong positive linear correlation with images from hyperpolarized xenon 129 (^{129}Xe) MRI (hereafter, ^{129}Xe MRI) ($\rho = 0.67$; $P < .001$) and technetium 99m–diethylenetriaminepentaacetic acid SPECT ventilation imaging (hereafter, V-SPECT) ($\rho = 0.65$; $P < .001$).
- The χ^2 distances of the ventilation histograms in the volume of interest between FAN and ^{129}Xe MRI (χ^2 distance, 0.16 ± 0.08) and FAN and V-SPECT (χ^2 distance, 0.28 ± 0.14) were small.
- The ratios of lobar ventilations in the FAN models were linearly correlated to the images from ^{129}Xe MRI ($\rho = 0.67$; $P < .001$) and V-SPECT ($\rho = 0.56$; $P < .001$).

with V-SPECT, extracting the information from this data-rich technique and understanding the nature of ventilation defects requires the use of numerical models (15), and to our knowledge, it has not yet been accepted into routine clinical practice.

Pulmonary structural information obtained from CT images has been used previously to develop patient-specific airway geometry in computational fluid dynamics studies (16,17). Furthermore, the application of mathematical algorithms enables modeling of the physiologic structured full-scale airways (18) and calculation of the airway flow beyond the limit of image resolution (19). A full-scale airway network (FAN) flow model (20) may also demonstrate the dynamic flow characteristics reported in earlier studies (21,22). Recently, the airway flow models have been improved by integrating poroelastic parenchymal flows (23) and gas transport (24). Our aim was to demonstrate a computational ventilation model by using CT structural imaging data and to compare this with functional lung imaging.

Materials and Methods

This prospective study was approved by the National Research Ethics Service Committee. All participants provided written informed consent (Research Ethics Committee approval number: 11/SC/0488). No industry support or funding was received for this study. The authors had full control of the data and information submitted for publication.

The participants with COPD were enrolled from a tertiary referral center between May 31 and August 31, 2017. The participants were imaged with multiple imaging modalities including CT, time-series ^{129}Xe MRI, and V-SPECT. Pulmonary function tests were performed on the same day as the examinations. Pulmonary function tests were performed according to American Thoracic Society/European Respiratory Society guidelines (25).

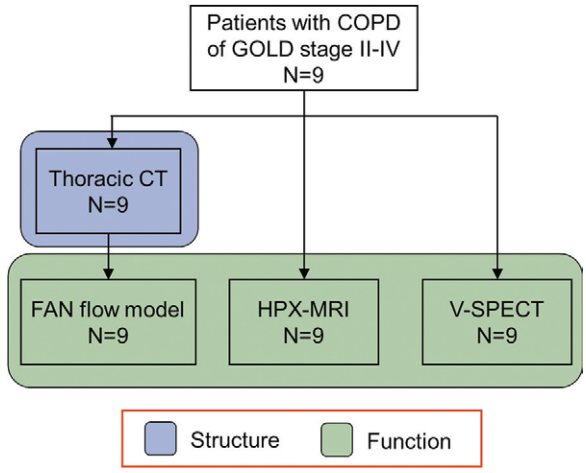

Figure 1: Schematic diagram of the study information flow and analysis. Structural data (lobes, large airways, and tissue density) from thoracic CT images in nine participants were used to build the full-scale airway network (FAN) flow model geometries and to determine the initial conditions. FAN-modeled ventilation was comparted with the hyperpolarized xenon 129 MRI (HPX-MRI) and technetium 99m–diethylenetriaminepentaacetic acid aerosol SPECT ventilation imaging (V-SPECT) data. COPD = chronic obstructive pulmonary disease, GOLD = Global Initiative for Chronic Obstructive Lung Disease.

Study Design

Figure 1 illustrates the summary of information flow within our study. Structural data including lobes, large airways (up to subsegmental bronchi generation eight), and tissue density of lungs obtained on CT images in participants were used in the FAN flow model. To enable the participant-specific characterization to simulate the breath-hold gas distribution, the participants' pulmonary function test results were used to determine the initial and boundary conditions of the flow and pressure. The computed ventilation distributions in the CT-based FAN models were compared with the corresponding participants' ^{129}Xe MRI and V-SPECT.

^{129}Xe MRI Technique and Analysis

To perform the ^{129}Xe MRI, a 1-L bag of 87% nuclear-enriched ^{129}Xe gas was polarized to 10%–15% in a commercial polarizer (Model 9300; Polarean, Durham, NC). The polarization level was measured with a commercial polarization measurement station (Model 2881, Polarean). The images were acquired by using a 1.5-T ^{129}Xe MRI system (Signa HDx; GE Healthcare, Milwaukee, Wis). MRI pulse sequence was as follows: repetition time msec/echo time μsec, 23/50. Time-series images were acquired on 13 coronal sections by using a flexible vest-shaped transmit-receive radiofrequency coil (Clinical MR Solutions, Brookfield, Wis) at ^{129}Xe MRI. The section thickness and field of view were 15 mm and 32 cm, respectively. For a 20-second breath hold, the time series ^{129}Xe MRI acquired eight sets of volume images by using eight interleaved spiral k-space sampling (26). The imaging temporal resolution was about 2.5 seconds and the spatial resolution of each section was 1–3 mm. The time-series ^{129}Xe MRI enabled quantification of relative lobar ventilation ratios similar to relative ventilation measured at SPECT as previously described (15).

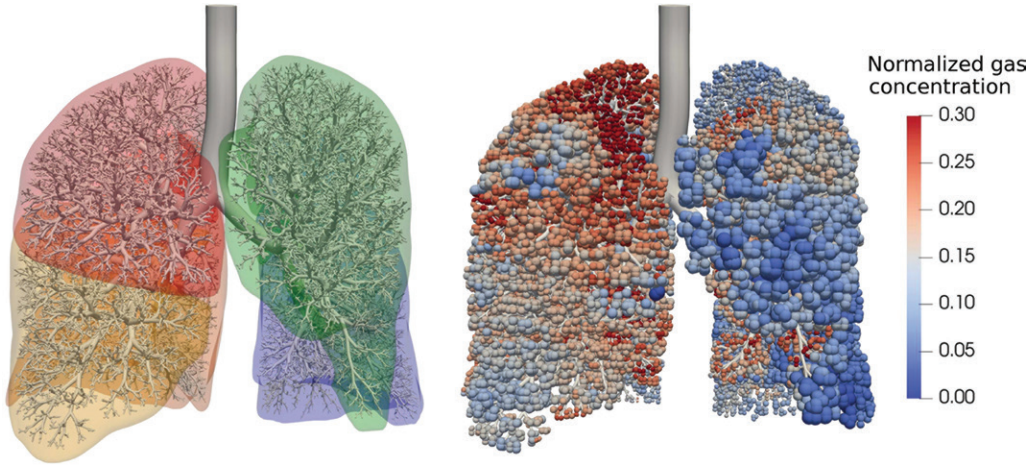

Figure 2: Illustration of the thoracic CT-based full-scale airway network flow model geometry of participant 1 (ParaView v5.5.2; Kitware, Clifton Park, NY). Each acinar unit shown as a sphere at the terminal bronchiole is interconnected with other units through the airway network. The size and color of spheres represent the scaled acinar volume and normalized acinar gas concentration. The color on the left-hand side of the image shows a lobe surface (red, right upper lobe; orange, right middle lobe; pink, right lower lobe; green, left upper lobe; purple, left lower lobe).

Characteristics of Study Participants

Participant No.	Age (y)	Sex	Height (cm)	Weight (kg)	GOLD stage	RV (L)	TLC (L)	FEV_1 (% predicted)	FEV_1/FVC (% predicted)
1	58	F	157	66.0	II	2.8	5.6	57	68
2	73	M	163	55.0	IV	5.6	7.8	25	37
3	64	M	185	128.2	II	2.5	7.4	63	75
4	68	F	150	47.0	III	4.8	6.3	30	47
5	58	M	156	54.7	II	3.5	6.6	47	57
6	67	M	177	77.9	III	3.7	8.1	46	51
7	64	M	174	91.8	III	4.7	8.9	41	49
8	62	M	171	71.3	II	2.8	7.2	63	63
9	65	M	150	51.0	III	5.9	7.9	46	51
Overall*	64 ± 5		165 ± 12.5	71.4 ± 25.7		4.0 ± 1.2	7.3 ± 1.0	46.4 ± 13.3	55.3 ± 11.7

Note.—FEV_1 = forced expiratory volume in 1 second, FVC = forced vital capacity, GOLD = Global Initiative for Chronic Obstructive Lung Disease, RV = residual volume, TLC = total lung capacity.

* Mean data are ± standard deviation.

Computational Modeling and Data Analysis

The surface geometries of pulmonary lobes and large airways until fifth to eighth generation were segmented from CT images by using an open-access software (Pulmonary Toolkit; *https://github.com/tomdoel/pulmonarytoolkit*) (27). Moreover, the software (Pulmonary Toolkit) extracted the centerlines of the segmented airways and tissue density data from CT. The tissue density was assessed by using Hounsfield units and the densities of air and water were assessed at standard temperature (0°C) and pressure (100 kPa) (28). A branch-growing algorithm in an open-source library for computational physiology and biology (Chaste; *https://github.com/Chaste/Chaste/releases/tag/release_2017.1*) was applied to generate anatomically structured small airways filling the lobes (18). Maximum generation numbers of the full-scale airways were 25–27 and approximately 30 000 terminal bronchioles were created (Fig 2). The tissue density data and lung volume information (residual volume and total lung capacity) were used to determine the initial acini volumes at the end of terminal bronchioles in the model (28). In addition to the dynamic pressure and flow solving in an airway network system with the FAN model (20,29), we included a function to estimate dynamic gas concentration changes in each airway element. The FAN model code will be available from the authors on request. Gas concentration projected on a coronal plane from the model was compared with the corresponding ventilation distributions obtained from ^{129}Xe MRI and V-SPECT in nine participants with COPD. To determine the clinical nature of individual ventilation distributions, lobar defects in ventilation detection by using the FAN model, ^{129}Xe MRI, and V-SPECT were compared by three authors (M.K.; O.D.; and T.N.M., with 8 years of clinical radiology experience) with the areas with attenuation values of less than −950 HU of the corresponding lobes (13,30,31) obtained by open-access software (Pulmonary Toolkit) (32). In addition, the ventilation distribution was integrated from the anterior-to-posterior direction and the correlations of the line profiles at different elevations of lungs were assessed between the FAN model and ^{129}Xe MRI and V-SPECT for quantitative comparison. Moreover, the characteristics of ventilation distri-

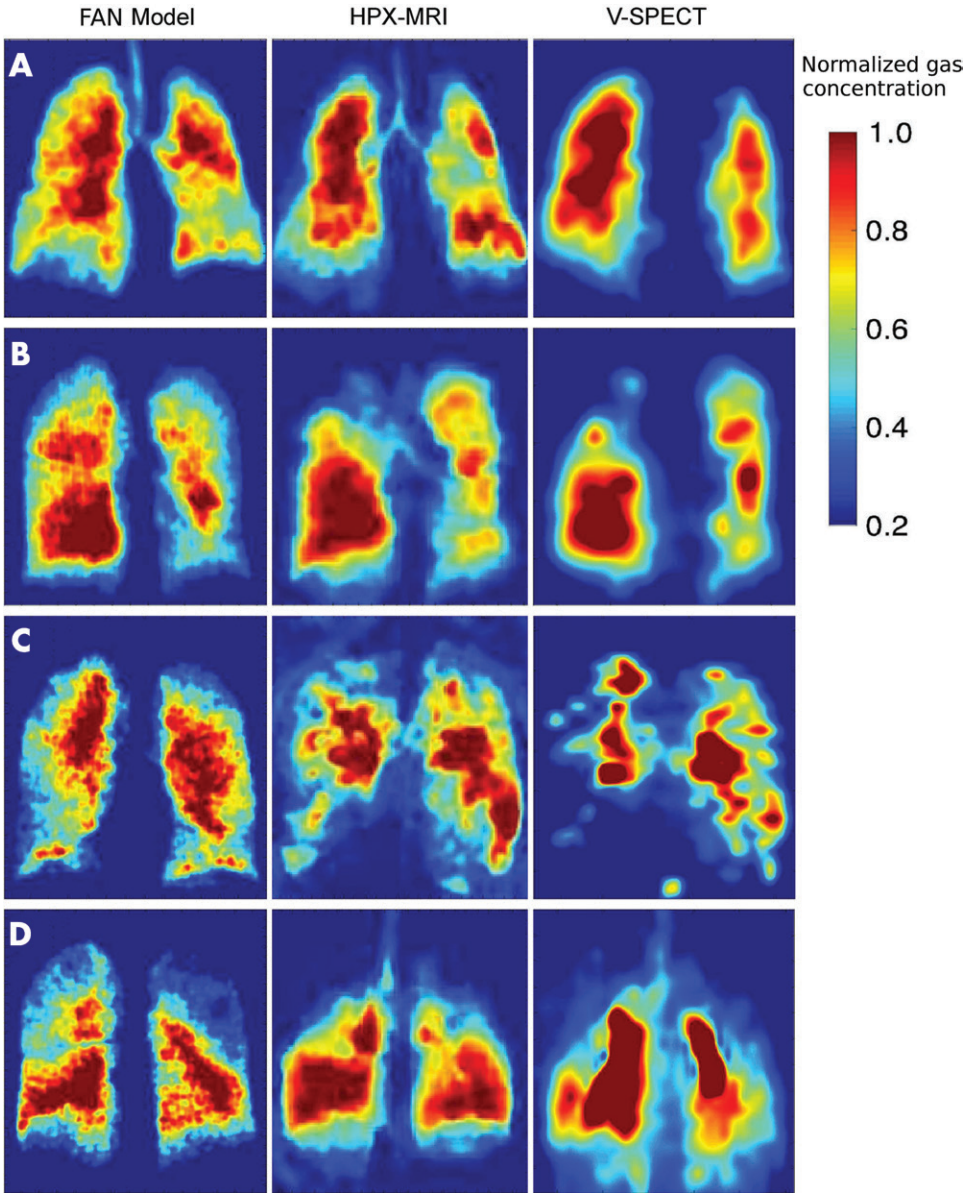

Figure 3: Ventilation distribution projected on a coronal plane in four participants (*A–D*). Full-scale airway network (FAN) models demonstrate computed gas concentrations whereas hyperpolarized xenon 129 MRI (HPX-MRI) and technetium 99m–diethylenetriaminepentaacetic acid aerosol SPECT ventilation imaging (V-SPECT) show the ventilations assessed from signal intensity. The additional factors affecting HPX signal except gas concentration were filtered out by using the signal-time curve fitting technique. Antialiasing was performed by using bicubic interpolation to resize the V-SPECT data.

butions within four volumes of interest defined to be consistent across different modalities of each lung were illustrated on probability histograms. The relative percentage gas ventilations were also calculated for each lobe to compare regional ventilation rates between the model and functional imaging.

Details of CT analysis including the areas with low attenuation values (less than −950 HU), V-SPECT technique, and gas concentration modeling with FAN are in Appendix E1 (online).

Statistical Analysis

Spearman correlation coefficient was calculated to compare the line profiles of ventilation distribution between FAN model and functional images. The similarities of the two histograms were assessed by using χ^2 distances. *P* values less than .05 were considered to indicate statistical significance. Statistical analyses were performed by using statistical software (Matlab version R2018b; MathWorks, Natick, Mass).

Results

Study Cohort Demographics

Nine participants with COPD were included on the basis of the following inclusion criteria: the Global Initiative for Chronic Obstructive Lung Disease, known as GOLD, criteria, stages II–IV (forced expiratory volume in 1 second, 80% predicted and forced expiratory volume in 1 second/forced vital capacity, 70%); substantial smoking history (>15 pack-years); age older than 18 years; and ability to provide informed consent. Seven participants were men (mean age, 65 years ± 5 [standard deviation]) and two participants were women (mean age, 63 years ± 7). The summary of participant demographics and lung function is shown in the Table.

Ventilation Distribution

Figure 3 provides examples of the coronal pulmonary ventilation distributions generated by the model and demonstrated at ^{129}Xe MRI and V-SPECT for participants 1–4. The ventilation distribution patterns between participants were variable, which is consistent with their known heterogeneous disease. The ventilation distributions determined by using the CT-based FAN model showed a close resemblance to those depicted at ^{129}Xe MRI and V-SPECT. To investigate the similarity and differences between ^{129}Xe MRI, V-SPECT, and the CT-based FAN model in Figure 3, the line profiles were compared in Figure 4.

Ventilation profiles from the CT-based FAN model, ^{129}Xe MRI, and V-SPECT (Fig 3) are demonstrated in Figure 4 at different levels (L1–L6). Figure 4a shows the ventilation profiles in participants 5–7. The ventilation profiles measured from the FAN model showed a strong positive correlation to those from the functional imaging (ie, ^{129}Xe MRI

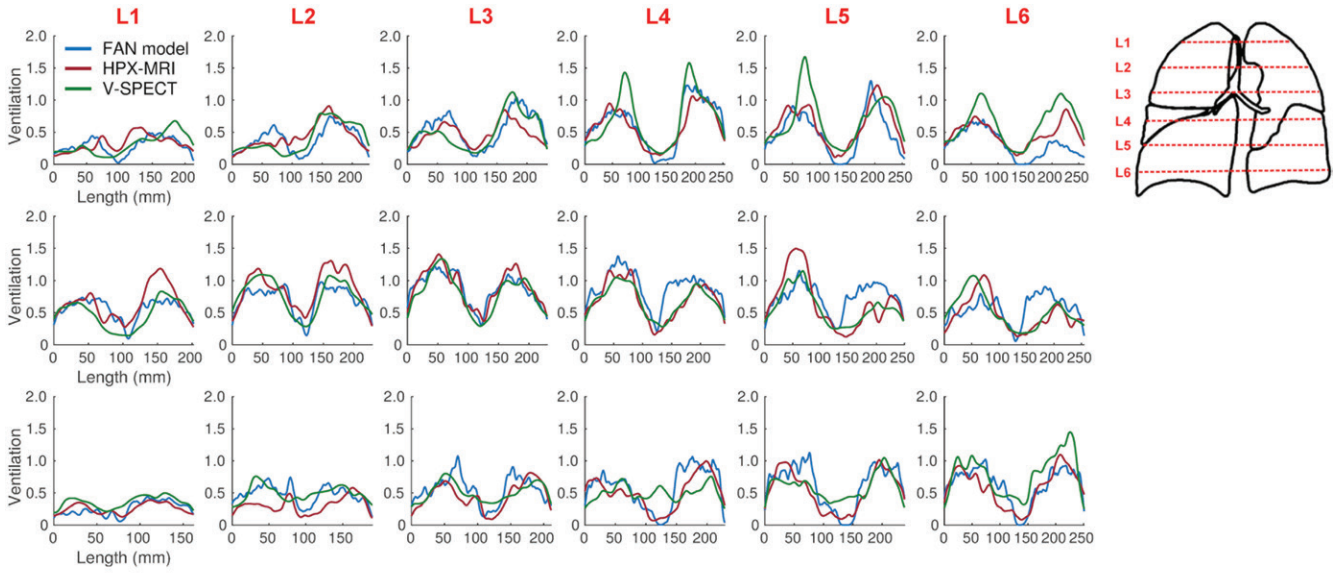

a.

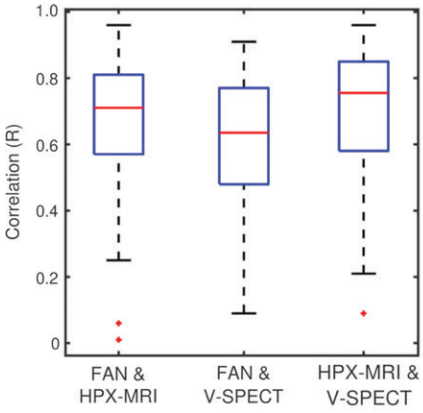

b.

Figure 4: **(a)** Comparison of ventilation profiles at different elevations (L1–L6) in participants 5–7. **(b)** Box-and-whisker plots of the Spearman correlations of ventilation profiles in participants overall. The correlation between the full-scale airway network (FAN) model and hyperpolarized xenon 129 MRI (HPX-MRI) is comparable to the HPX-MRI and technetium 99m–diethylenetriaminepentaacetic acid aerosol SPECT ventilation imaging (V-SPECT) pair.

and V-SPECT). The overall correlations for all participants included in the study are provided in Figure 4b. The data in the space between right and left lungs were excluded when assessing the correlations. Median Spearman correlation coefficients between the FAN and ^{129}Xe MRI, FAN and V-SPECT, and ^{129}Xe MRI and V-SPECT (with first and third quartiles in parentheses) were as follows: $\rho = 0.67$ (0.58, 0.81; $P < .001$), $\rho = 0.65$ (0.48, 0.77; $P < .001$), and $\rho = 0.75$ (0.58, 0.85; $P < .001$), respectively.

The characteristics of ventilation distribution in the volumes of interest in participant 6 are shown in Figure 5a. All histograms of the normalized ventilation probability obtained from the FAN model, ^{129}Xe MRI, and V-SPECT showed right-skewed distributions. The χ^2 distance assessing the difference between two histograms showed a close similarity between the FAN model and ^{129}Xe MRI and V-SPECT in the right (R1, R2) and the left upper (L1) volumes of interest in the participant 6. The ventilation histogram assessed by the FAN model showed closer similarity to the ^{129}Xe MRI than the V-SPECT in all volumes except the right lower (R2) volume of interest. Figure 5b illustrates the overall χ^2 distances showing the difference in volume-of-interest ventilation distribution between FAN model and images. The mean of the χ^2 distance showed that the FAN model and ^{129}Xe MRI (χ^2 distance, 0.16 ± 0.08) had better agreement in ventilation distribution than other comparison pairs (FAN and V-SPECT χ^2 distance, 0.28 ± 0.14; ^{129}Xe MRI and V-SPECT χ^2 distance, 0.24 ± 0.15).

Figure 6 shows the lobar ventilation ratios assessed from the FAN model, ^{129}Xe MRI, and V-SPECT. The linear regression plots of the lobar ventilation ratios showed that there were strong positive correlations between the model and the imaging data sets. The correlation between the model and ^{129}Xe MRI was stronger than the model and V-SPECT correlation. Accordingly, the coefficients of Spearman correlation between the FAN and ^{129}Xe MRI, FAN and V-SPECT, and ^{129}Xe MRI and V-SPECT were $\rho = 0.67$ ($P < .001$), $\rho = 0.59$ ($P < .001$), and $\rho = 0.63$ ($P < .001$), respectively.

Discussion

Thoracic CT can provide valuable insight into lung structure, but the lack of functional information remains a limitation at the clinical diagnosis. Our study demonstrates the successful assessment of pulmonary ventilation in participants with chronic obstructive pulmonary disease (COPD) by using a CT-based full-scale airway network (FAN) flow model. The ventilation profile simulated by the FAN showed a strong positive correlation with hyperpolarized xenon 129 (^{129}Xe) MRI (hereafter, referred to as ^{129}Xe MRI; median $\rho = 0.67$; $P < .001$) and technetium 99m–diethylenetriaminepentaacetic acid aerosol SPECT ventilation imaging (hereafter, referred to as V-SPECT; median $\rho = 0.65$; $P < .001$).

For improved participant specificity, the FAN model used tissue density, lung volumes, and pulmonary function test

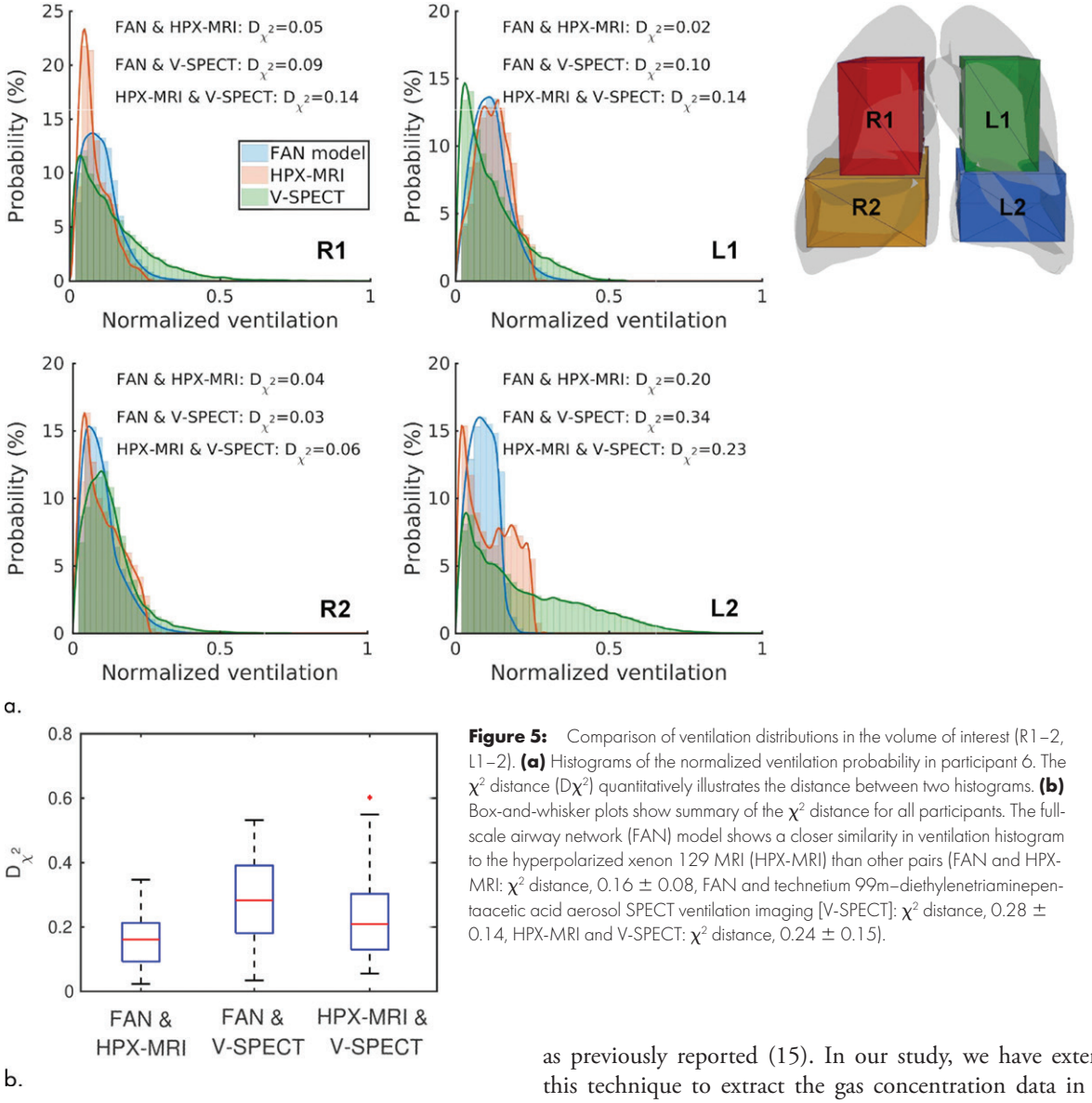

Figure 5: Comparison of ventilation distributions in the volume of interest (R1–2, L1–2). **(a)** Histograms of the normalized ventilation probability in participant 6. The χ^2 distance (Dχ^2) quantitatively illustrates the distance between two histograms. **(b)** Box-and-whisker plots show summary of the χ^2 distance for all participants. The full-scale airway network (FAN) model shows a closer similarity in ventilation histogram to the hyperpolarized xenon 129 MRI (HPX-MRI) than other pairs (FAN and HPX-MRI: χ^2 distance, 0.16 ± 0.08, FAN and technetium 99m–diethylenetriaminepentaacetic acid aerosol SPECT ventilation imaging [V-SPECT]: χ^2 distance, 0.28 ± 0.14, HPX-MRI and V-SPECT: χ^2 distance, 0.24 ± 0.15).

results in addition to hybrid geometry of large and small airways to determine the initial and boundary conditions of the model for each individual. The network airway flow characteristics were different from flows in an isolated system (22,33). The FAN model interactively connected all acini units through the airway network enabling simulation of complex flow behavior because of asymmetric physiologic airway structure (20). To assess the inspired gas transfer mixing with air and to compare with the functional imaging data, we included solving gas concentration in addition to the original network airflow solver. The ventilation distribution generated by the FAN model correlated with those detected at ^{129}Xe MRI and V-SPECT. This is the first study, to our knowledge, to demonstrate successful full-scale assessment of pulmonary ventilation distribution by using a network airway flow model that correlates with functional imaging.

We demonstrated a strong correlation between relative lobar percentage ventilation detected at ^{129}Xe MRI and V-SPECT, as previously reported (15). In our study, we have extended this technique to extract the gas concentration data in each voxel from the ^{129}Xe MRI signal. We improved the assessment of ventilation by using ^{129}Xe MRI by minimizing interference from the known additional factors affecting it (the choice of k-space sampling and radiofrequency coil characteristics) (29,31), which allowed a more accurate comparison between the functional imaging modalities. The analysis of ventilation according to individual voxels presents an opportunity for increased detail and accuracy in assessment of ventilation heterogeneity by using ^{129}Xe MRI that is not otherwise possible with lower spatial-resolution imaging modalities.

In a recent quantitative image analysis study, Tahir et al (34) demonstrated a strategy of image acquisition and analysis to assess lung ventilation on breath-hold CT images. They found the spatial correlations between the different image modalities, CT ventilation and ^{129}Xe MRI, were strong (ρ = 0.6–0.7) for the best case. Our study compared a computational model and images. The median Spearman correlations between the CT-based FAN model and ^{129}Xe MRI were significant (ρ = 0.67) for both the ventilation profiles and the lobar ventilation ratio. Additionally, our FAN model demonstrated close similarity of

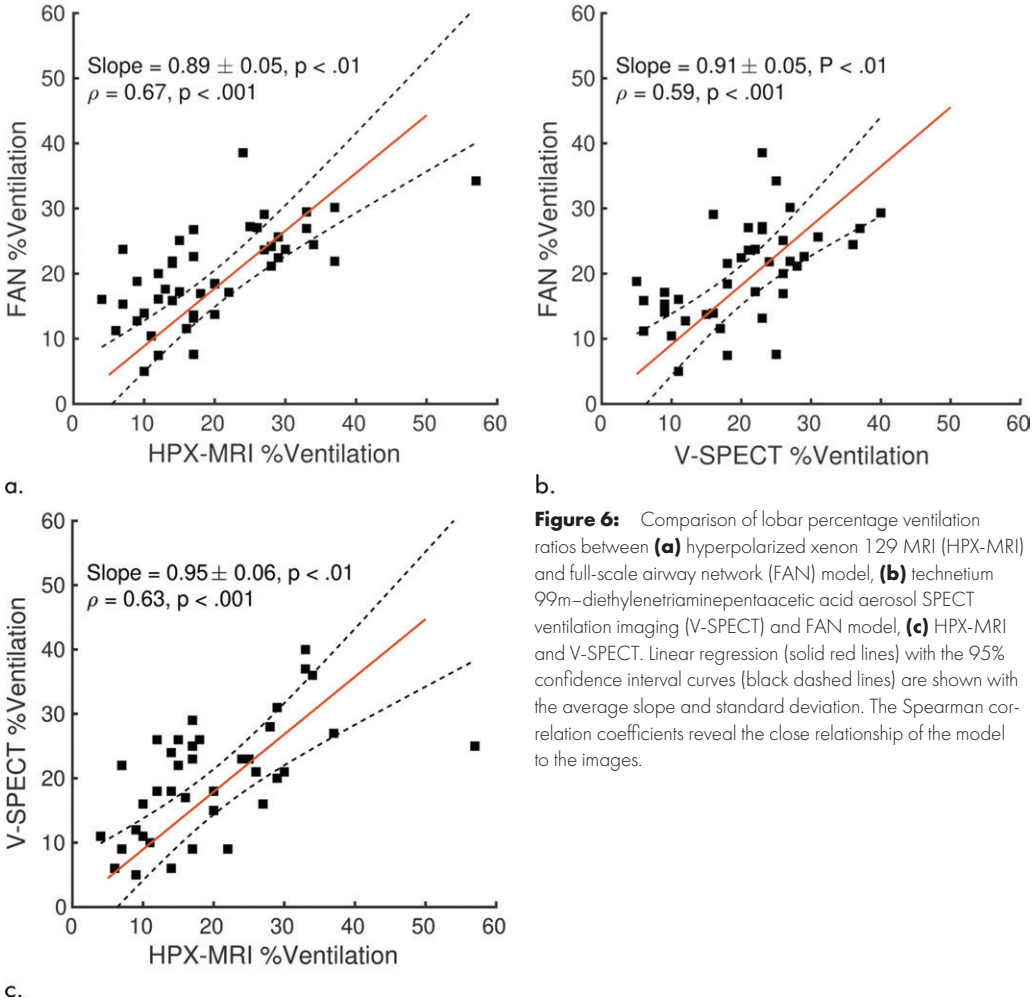

Figure 6: Comparison of lobar percentage ventilation ratios between **(a)** hyperpolarized xenon 129 MRI (HPX-MRI) and full-scale airway network (FAN) model, **(b)** technetium 99m–diethylenetriaminepentaacetic acid aerosol SPECT ventilation imaging (V-SPECT) and FAN model, **(c)** HPX-MRI and V-SPECT. Linear regression (solid red lines) with the 95% confidence interval curves (black dashed lines) are shown with the average slope and standard deviation. The Spearman correlation coefficients reveal the close relationship of the model to the images.

the ventilation distribution in the volumes of interest with the ^{129}Xe MRI data and showed better agreement with ^{129}Xe MRI than V-SPECT. This may be explained by the relatively lower spatial resolution of V-SPECT compared with ^{129}Xe MRI that affects the comparisons, because our model provides more detailed information on ventilation distribution, and we have previously reported on the relationship between ^{129}Xe MRI and V-SPECT (15).

Ventilation defects observed with ^{129}Xe MRI are caused by a variety of physiologic factors, including the heterogenous gas distribution because of bronchial constriction or obstruction and/or the poor gas concentration within the alveolar airspace from emphysematous tissue destruction. Our FAN model incorporated both of these participant-specific characteristics: the airway structure up to the fifth through eighth generations of sub-bronchi and parenchymal tissue density at CT. Nonetheless, the influence of small airway obstruction and constriction was not within the scope of our model. Thus, the difference between the FAN model and the functional imaging may be because of the presence of small airway obstruction, which is beyond the sub-bronchial determination from our model. Additionally, poroelastic flow and parenchymal gas diffusion are not included in the current FAN model and remain an area for future research.

Although we demonstrated good statistical correlations, these may have been affected by the within-participant data sampling, and before the FAN model is used in clinical practice it will require further investigation in studies with a substantially larger number of participants.

In future studies, it would be useful to compare the FAN model ventilation distributions with other ^{129}Xe MRI sequences including apparent diffusion coefficient for evaluation of pulmonary microstructure and dissolved phase imaging to assess gas transfer and exchange. The information obtained from both methods may complement each other and would allow for a more comprehensive assessment of lung function than is currently possible.

In conclusion, our study successfully demonstrated pulmonary ventilation distribution generated by a patient-specific full-scale airway network flow model that correlated with hyperpolarized xenon 129 MRI and technetium 99m–diethylenetriaminepentaacetic acid aerosol SPECT ventilation imaging. The full-scale airway network flow model has the potential to provide valuable insights into regional ventilation and dynamic airflow in a variety of lung diseases.

Author contributions: Guarantors of integrity of entire study, M.K., O.D., F.V.G.; study concepts/study design or data acquisition or data analysis/interpretation, all authors; manuscript drafting or manuscript revision for important intellectual content, all authors; approval of final version of submitted manuscript, all authors; agrees to ensure any questions related to the work are appropriately resolved, all authors; literature research, M.K., O.D., T.N.M.; clinical studies, O.D., T.N.M., F.V.G.; experimental studies, M.K., O.D., T.P.; statistical analysis, M.K., O.D., T.P.; and manuscript editing, all authors

Disclosures of Conflicts of Interest: **M.K.** disclosed no relevant relationships. **O.D.** disclosed no relevant relationships. **T.N.M.** disclosed no relevant relationships. **T.P.** disclosed no relevant relationships. **F.V.G.** disclosed no relevant relationships.

References

1. GBD 2015 Chronic Respiratory Disease Collaborators. Global, regional, and national deaths, prevalence, disability-adjusted life years, and years lived with disability for chronic obstructive pulmonary disease and asthma, 1990-2015: a systematic analysis for the Global Burden of Disease Study 2015. Lancet Respir Med 2017;5(9):691–706.
2. Vestbo J, Hurd SS, Agustí AG, et al. Global strategy for the diagnosis, management, and prevention of chronic obstructive pulmonary disease: GOLD executive summary. Am J Respir Crit Care Med 2013;187(4):347–365.
3. Müller NL, Coxson H. Chronic obstructive pulmonary disease. 4: imaging the lungs in patients with chronic obstructive pulmonary disease. Thorax 2002;57(11):982–985.
4. Kuwano K, Matsuba K, Ikeda T, et al. The diagnosis of mild emphysema. Correlation of computed tomography and pathology scores. Am Rev Respir Dis 1990;141(1):169–178.
5. Wang Z, Gu S, Leader JK, et al. Optimal threshold in CT quantification of emphysema. Eur Radiol 2013;23(4):975–984.
6. Rabe KF, Hurd S, Anzueto A, et al. Global strategy for the diagnosis, management, and prevention of chronic obstructive pulmonary disease: GOLD executive summary. Am J Respir Crit Care Med 2007;176(6):532–555.
7. Cerveri I, Dore R, Corsico A, et al. Assessment of emphysema in COPD: a functional and radiologic study. Chest 2004;125(5):1714–1718.
8. Labaki WW, Martinez CH, Martinez FJ, et al. The Role of Chest Computed Tomography in the Evaluation and Management of the Patient with Chronic Obstructive Pulmonary Disease. Am J Respir Crit Care Med 2017;196(11):1372–1379.
9. Jögi J, Ekberg M, Jonson B, Bozovic G, Bajc M. Ventilation/perfusion SPECT in chronic obstructive pulmonary disease: an evaluation by reference to symptoms, spirometric lung function and emphysema, as assessed with HRCT. Eur J Nucl Med Mol Imaging 2011;38(7):1344–1352.
10. Petersson J, Sánchez-Crespo A, Larsson SA, Mure M. Physiological imaging of the lung: single-photon-emission computed tomography (SPECT). J Appl Physiol (1985) 2007;102(1):468–476.
11. Adamson EB, Ludwig KD, Mummy DG, Fain SB. Magnetic resonance imaging with hyperpolarized agents: methods and applications. Phys Med Biol 2017;62(13):R81–R123.
12. Collier GJ, Wild JM. In vivo measurement of gas flow in human airways with hyperpolarized gas MRI and compressed sensing. Magn Reson Med 2015;73(6):2255–2261.
13. Matin TN, Rahman N, Nickol AH, et al. Chronic Obstructive Pulmonary Disease: Lobar Analysis with Hyperpolarized 129Xe MR Imaging. Radiology 2017;282(3):857–868.
14. Virgincar RS, Cleveland ZI, Kaushik SS, et al. Quantitative analysis of hyperpolarized 129Xe ventilation imaging in healthy volunteers and subjects with chronic obstructive pulmonary disease. NMR Biomed 2013;26(4):424–435.
15. Doganay O, Matin T, Chen M, et al. Time-series hyperpolarized xenon-129 MRI of lobar lung ventilation of COPD in comparison to V/Q-SPECT/CT and CT. Eur Radiol 2019;29(8):4058–4067.
16. Kim M, Collier GJ, Wild JM, Chung YM. Effect of upper airway on tracheobronchial fluid dynamics. Int J Numer Methods Biomed Eng 2018;34(9):e3112.
17. Oakes JM, Mummy D, Poorbahrami K, Zha W, Fain SB. Patient-Specific Computational Simulations of Hyperpolarized 3He MRI Ventilation Defects in Healthy and Asthmatic Subjects. IEEE Trans Biomed Eng 2018.
18. Bordas R, Lefevre C, Veeckmans B, et al. Development and analysis of patient-based complete conducting airways models. PLoS One 2015;10(12):e0144105.
19. Ismail M, Comerford A, Wall WA. Coupled and reduced dimensional modeling of respiratory mechanics during spontaneous breathing. Int J Numer Methods Biomed Eng 2013;29(11):1285–1305.
20. Kim M, Bordas R, Vos W, et al. Dynamic flow characteristics in normal and asthmatic lungs. Int J Numer Methods Biomed Eng 2015;31(12):e02730.
21. Otis AB, McKerrow CB, Bartlett RA, et al. Mechanical factors in distribution of pulmonary ventilation. J Appl Physiol 1956;8(4):427–443.
22. Greenblatt EE, Butler JP, Venegas JG, Winkler T. Pendelluft in the bronchial tree. J Appl Physiol (1985) 2014;117(9):979–988.
23. Berger L, Bordas R, Burrowes K, Grau V, Tavener S, Kay D. A poroelastic model coupled to a fluid network with applications in lung modelling. Int J Numer Methods Biomed Eng 2016;32(1):e02731.
24. Foy BH, Kay D. A computational comparison of the multiple-breath washout and forced oscillation technique as markers of bronchoconstriction. Respir Physiol Neurobiol 2017;240:61–69.
25. Miller MR, Crapo R, Hankinson J, et al. General considerations for lung function testing. Eur Respir J 2005;26(1):153–161.
26. Doganay O, Matin TN, Mcintyre A, et al. Fast dynamic ventilation MRI of hyperpolarized ^{129}Xe using spiral imaging. Magn Reson Med 2018;79(5):2597–2606.
27. Doel T. The pulmonary toolkit. https://github.com/tomdoel/pulmonarytoolkit. Accessed December 10, 2018.
28. Burrowes KS, Doel T, Kim M, et al. A combined image-modelling approach assessing the impact of hyperinflation due to emphysema on regional ventilation–perfusion matching. Comput Methods Biomech Biomed Eng Imaging Vis 2015;5(2):110–126.
29. Kim M. Full-scale airway network flow model V0.0.9. https://github.com/peter3k/FAN-flow-model.git. Accessed August 6, 2019.
30. Kirby M, Svenningsen S, Owrangi A, et al. Hyperpolarized 3He and 129Xe MR imaging in healthy volunteers and patients with chronic obstructive pulmonary disease. Radiology 2012;265(2):600–610.
31. Kirby M, Svenningsen S, Kanhere N, et al. Pulmonary ventilation visualized using hyperpolarized helium-3 and xenon-129 magnetic resonance imaging: differences in COPD and relationship to emphysema. J Appl Physiol (1985) 2013;114(6):707–715.
32. Doel T, Matin TN, Gleeson FV, Gavaghan DJ, Grau V. Pulmonary lobe segmentation from CT images using fissureness, airways, vessels and multilevel B-splines. Proc IEEE Int Symp Biomed Imaging, Barcelona, Spain; 2012.
33. Winkler T, Venegas JG. Self-organized patterns of airway narrowing. J Appl Physiol (1985) 2011;110(5):1482–1486.
34. Tahir BA, Hughes PJC, Robinson SD, et al. Spatial comparison of CT-based surrogates of lung ventilation with hyperpolarized Helium-3 and Xenon-129 gas MRI in patients undergoing radiation therapy. Int J Radiat Oncol Biol Phys 2018;102(4):1276–1286.